Caving 2022 - Y Potvin (ed.)

doi:10.36487/ACG_repo/2205_31

Use of seismic tomography to aid rock mechanics interpretation at New Afton B3 block cave mine

C Kamp *New Gold Inc., Canada*

A Conley *New Gold Inc., Canada*

DS Collins *ESG Solutions, Canada*

M Preiksaitis *ESG Solutions, Canada*

T Butler *ESG Solutions, Canada*

V Shumila *ESG Solutions, Canada*

Abstract

New Gold's New Afton gold-copper mine is successfully mining different regions of the orebody using block caving. The present block cave at the mine, B3, successfully initiated steady state caving below the completed Lift 1 Block Cave in January 2022 with 8.8 MT (probable tonnes). Instrumentation monitoring methods in B3 include seismic event location, optical and metallic time-domain reflectometer (TDR), Elexon Geo4Sight and Elexon Beacons, and are being used to interpolate the 3D shape of the cave profile. For the first time at this mine, seismic tomography is being used to help interpret the stress and damage state of the rock mass around the cave.

This paper presents results from the seismic tomography and the interpretation of the high and low stress regions. Regions of rock mass destressing are determined in seismically active areas as well as aseismic zones. Tomographic velocity differences show that stress migration is occurring within certain regions of the abutments and above as the block cave growth progresses. The seismic tomography interpretation, accompanied by geological information and other geotechnical instrumentation, is helping to improve the safety and productivity of this mining operation.

Keywords: *seismicity, tomography, caving, stress, instrumentation, safety*

1 Introduction

An essential part of block cave mining is to accurately track the shape of the cave profile (yielded rock mass within the orebody induced by the caving process) to mitigate the risks of air blast, dilution, understand relationships with lithology and faulting, and recognise changes in induced stresses as the caved orebody progresses over the mining footprint. High stress regions in the rock mass have more potential of inducing damaging seismic events, while lower stress conditions are generally of less concern for mining and can be indicative of fully failed material or post-peak residual behaviour.

One of the challenges of cave mining is the lack of direct access to previously failed and mined-out zones compared to more conventional mining methods. Some of the key rock mass monitoring equipment used to help gain a better understanding of rock mass deformation at New Afton include microseismic sensors, metallic and optical TDR, and Elexon Beacons and Geo4Sight.

A well-designed microseismic array (Figure 1) can monitor the full 3D volume of the mine and cave and can provide a window into the rock mass behaviour. Seismic events can be located, and their spatial distribution, magnitude and other source characteristics analysed. The events can be further processed for the seismic moment tensor (SMT) which allows an understanding of the strain directions (pressure, tension axes) and the failure plane orientations. Seismic stress inversion can use a cluster of SMT results to solve for local stress

direction vectors. An additional advanced complimentary method is seismic tomography, a technique which helps to interpret relative stress magnitudes and changes over time as mining progresses.

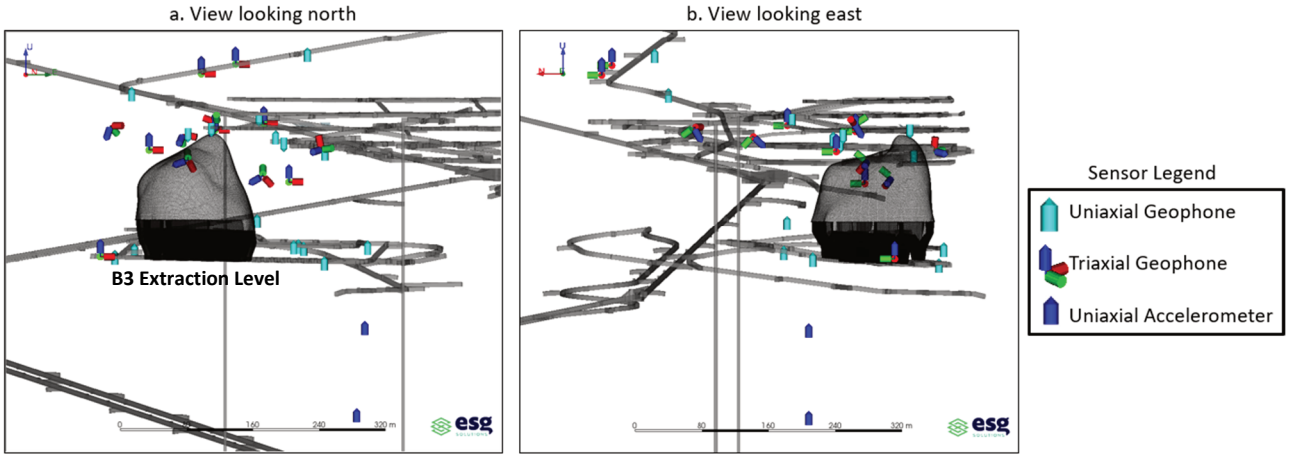

Figure 1 (a) View looking north and (b) View looking east of the New Afton B3 and an example interpreted cave profile (grey). The symbols depict the microseismic monitoring system, which consists of two uniaxial accelerometers, 16 uniaxial geophones and 13 triaxial geophones

Seismic tomography can utilise both induced seismicity (events), and blasts, if the seismic waveforms are accurately processed for arrival time and location. An advantage of seismic tomography is that information about seismically inactive regions of the rock mass can also be gained if there are source-sensor raypaths travelling through these regions. Areas of increasing stress show increasing seismic velocities since increased stress will result in the closing of joints, fractures, microcracks and pore space, all leading to an overall increasing stiffness of the rock. Decreasing seismic velocity can be interpreted as areas of stress relaxation/destressing and can also indicate areas of damaged rock (inelastic deformation) or post-peak rock failure.

Seismic tomography can work at different scales. Carlson et al. (1993), for example, showed the P-wave velocity tomography values to decrease as grain sized fractures formed on a 0.3 m diameter granite sample under thermal load. Using lower frequency sensors, Young and Maxwell (1992) showed that a moment magnitude (Mw) 2.0 event occurred within 10 m of the highest tomographic velocity region imaged at Strathcona stoping mine, suggesting high stress as the cause of the event. Maxwell and Young (1996) compared elastic stress modelling with seismic tomography results around a 3.5 m diameter horizontal tunnel at 420 m depth in Manitoba and showed a clear match of high velocity and high stress (where noticeable damage occurred at the tunnel perimeter), and low velocity and low stress (in the tensile regions perpendicular to sigma1).

More recently, Westman et al. (2008) used seismic tomography imaging to show high velocity (interpreted as high stress) ahead and to the sides of a longwall coal mining operation. Westman et al. (2012) applied seismic tomography to a block cave mine over an 18-month period and showed low velocity zones where the initial undercut was developed followed by high velocity (high stress) as the cave boundary increased upwards. De Beer et al. (2012) showed the change in tomographic velocity from high to low that occurred in time periods before and after a damaging 2.0 Mw event at San Rafael mine. Pfitzner et al. (2010) showed that preconditioning (hydraulic fracturing) in drill holes at Ridgeway Deeps block cave mine resulted in low tomographic velocity zones. As the cave developed at Ridgeway, the distribution of low velocity zones (cave) and high velocity zones (solid rock) in elevation above the undercut were used to help interpret the position of the cave and seismogenic zone above. Mercier et al. (2015) showed tomographic velocity images over a 24-month period at Northparkes block cave mine with initial seismicity generally occurring in a high velocity zone (high stress) with velocity decreasing over time in that zone. Viegas et al. (2018) applied velocity tomography along with other collective behaviour methods (Dynamic Parameter Analysis) to analyse a block cave mine and introduce the Vp/Vs ratio; tomographic P-wave velocity (Vp) / S-wave velocity (Vs), as a way

to interpret anisotropy in the rock mass. Baig et al. (2017) used tomography around a sill pillar in a hard rock mine. The sill initially showed a high velocity zone, which migrated and dispersed after the stope blast. De Beer et al. (2018) showed tomography results, seismic moment, and Energy Index results around a block cave mine and interpreted a stress cycling type behaviour. Ma et al. (2020) used tomographic imaging at Creighton stope mine to show the highest rate of seismicity corresponded to high velocity zones with the velocity decreasing over time. Afrouz & Westman (2018) produced an elastic stress model of a block cave and assigned velocity values corresponding to the stress level. They did raytracing, determined synthetic travel times and used tomography to reproduce closely the original velocity results, matching the high velocity to the high stress. They also highlighted the increased resolution with more raypaths used.

2 Geology and site overview

New Gold Inc. began construction and development of the New Afton Mine in 2007 and reached commercial production in July 2012 following the first drawbell blast in September 2011 on Lift 1 West Cave. The operation occupies the site of the historic Afton open pit mine, which operated from 1977 through 1997. The site includes an inactive and dewatered open pit and other historic facilities.

The principal commodities extracted at New Afton are gold and copper in concentrates. In 2021 and 2022, New Afton completed its first two Block Caves on Lift 1, the West and East Caves which mined over 24.5 MT and 23.7 MT respectively. Currently, New Afton successfully initiated and is monitoring steady state caving of B3 Cave in January 2022 with 8.8 MT (probable tonnes). Production involves milling over 8,000 tpd stemming from both the B3 Cave and a recovery level located below the East Cave. Decline drifts are currently being developed down to C-Zone to establish the C-Zone block cave, which comprises 29.5 MT (probable tonnes).

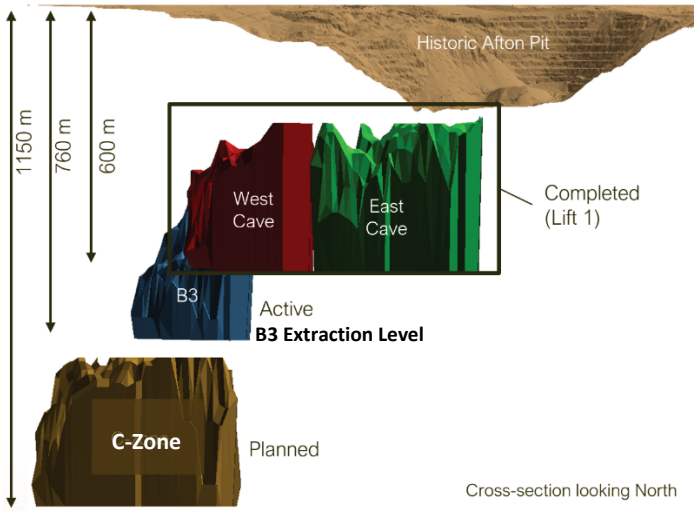

Figure 2 Cross-section view (mine grid north) of New Afton caves

The principal host lithologies for the mineralisation and production levels are crystalline and polymictic fragmental rocks and monomictic intrusive breccias, grouped together as a unit termed BXF, which primarily makes up the West, B3 and C-Zone Caves. In the eastern half of the deposit, specifically for the East Cave, the BXF is intruded by a diorite sill (DI). These units are bounded on the east by younger basalts and sedimentary rocks and bounded by an ultramafic picritic flow (PI) to the south. Monzonite (MO) bodies encompass both the BXF and DI and is interpreted to be a causative intrusive phase for mineralisation (Figure 3). In general, New Afton has a relatively low seismic velocity and highly attenuating rock mass due to the amount of geological structural influence within the orebody. For the Lift 1 block volume the average velocity was Vp = 4,980 m/s in February 2012, decreasing to Vp = 4,700 m/s in January 2013 as the cave developed (Collins et al. 2013). The B3 block volume, that was significantly more seismically active than the Lift 1 caves, had a Vp = 5,190 m/s in July 2021 (before caving developed) which is 4% higher than the Lift 1

block volume. The higher rate of seismicity at B3 is believed to be a combination of the slightly higher velocity (stronger rock mass), higher stress acting (deeper), and less attenuating rock mass, however the higher microseismic sensor density could be a significant factor causing this observation.

Figure 3 B3 Extraction Level, 16.5 × 27.0 m drawpoint spacing, faults and lithology shown

3 Instrumentation

3.1 Seismic system evolution

In May of 2008 a first approach of the seismic system design was completed for Lift 1. The original seismic network design was a full 1 V/g accelerometer array, consisting of 48 uniaxial and eight triaxial accelerometers. The system was designed to detect events induced from caving and to be cost efficient. Event location accuracy and system sensitivity was enhanced with the inclusion of more recording points (uniaxial sensors), while sufficient triaxial sensors were installed to obtain accurate seismic source parameters so that higher order data analysis techniques could be employed.

During 2009, the requirements of the seismic system were revisited due to the concern about high attenuation in parts of the rock mass. A revision to the array was produced in March 2011, consisting of a mixture of 21 × 1 V/g uniaxial accelerometers and 11 × 15 Hz triaxial geophones. Some of the sensors were also designed to be sacrificial and were installed within the expected caving area to provide better intersensory spacing to account for the attenuating rock mass. This would allow the seismic array to capture initial cave induced seismicity for the establishment of critical hydraulic radius (HRCrit), which is the critical hydraulic radius span required for yielding of the orebody, leading to steady state cave mine production, and observing cave monitoring instrument responses in the orebody.

In 2019, the B3 seismic system array was designed with lessons learned from the Lift 1 system in mind. With B3 being a shorter mining lift of 160 m and only 250 m long × 125 m wide, and with installation access directly above from the West Cave, there was an opportunity to install a strategic and closely spaced seismic monitoring system. The installed array consists of 16 × 15 Hz uniaxial geophones, 13 × 15 Hz triaxial geophones and 2 × 30 V/g accelerometers, with approximately 30–40% of the sensors being planned as sacrificial (installed within the minable orebody). Geophones were selected as the sensor of choice due to the waveform signal attenuation observed with the Lift 1 system. The B3 volume is deeper and in a similar rock mass to the overlying the Lift 1 West Cave but contains an increased occurrence of faulting than West Cave (Table 1).

The B3 microseismic system was commissioned gradually between February and July 2021 with the full system monitoring since August 2021. In comparison to Lift 1, B3 has provided a significant seismic event frequency for the similar milestones of cave start-up to steady state caving, providing enough quality seismic data to conduct additional seismic analysis such as passive seismic tomography.

Table 1 RMR'89 of the mining resource block estimated from core logging, with face mapping of the extraction level (in brackets)

Parameter		Cave footprint		
		West Cave	East Cave	B3 Cave
RQD	Median	75	63	78
(%)	25th percentile	60	43	65
	75th percentile	87	78	89
	Median	66 (50)	58 (45)	68 (52)
RMR'89	25th percentile	58 (45)	47 (37)	60 (47)
	75th percentile	72 (55)	66 (50)	74 (56)

3.1.1 Tomography methodology and analysis

With the collection of a reasonable amount of microseismic data (seismic events, blasts and noise), it was decided that an attempt at seismic tomography would be worthwhile with the data. The simultaneous iterative reconstruction technique (SIRT) tomography algorithm is used, as described in Crowley et al. (2015). The velocity range is constrained to be within predetermined acceptable values. This velocity range was set to be +/-30% from the starting values. The starting velocity model used is Vp = 5,190 m/s and was determined using the accurate picking of 14 blasts recorded with known locations.

A quality estimation called 'variance' is calculated for each grid cell based on the square root of diagonal elements in the inverse Fisher matrix. This quality estimation is useful because it is affected by the raypath coverage through a cell, as well as the quality of picking/processing, and the assumption that the velocity is constant during each selected time period. A benefit of the variance calculation is that velocity tomography images can be presented with high variance points removed. This exclusion removes velocity values of grid cells that have high uncertainty such as those with no raypaths or a low number of raypaths. For this study, the Vp results are shown if variance < 50%.

Tomographic imaging methods can resolve spatial heterogeneities of a medium that are larger than the wavelength of the seismic waves. The grid cell size was set to 50 m which assumes that all data used has some frequency content at 100 Hz and higher. Based on the sensor frequency range (15–1,000 Hz) and the average corner frequencies observed (~100 Hz), this is a reasonable assumption. Tomography results are presented with mild Gaussian smoothing to help focus on the significant trends in the data.

3.2 Other geotechnical instrumentation

Instrumentation monitoring methods in B3 include seismic event location, metallic and optical time-domain reflectometry (MTDR and OTDR), and Elexon Geo4Sight and beacons, which are being used to interpolate a 3D cave profile (Figure 4).

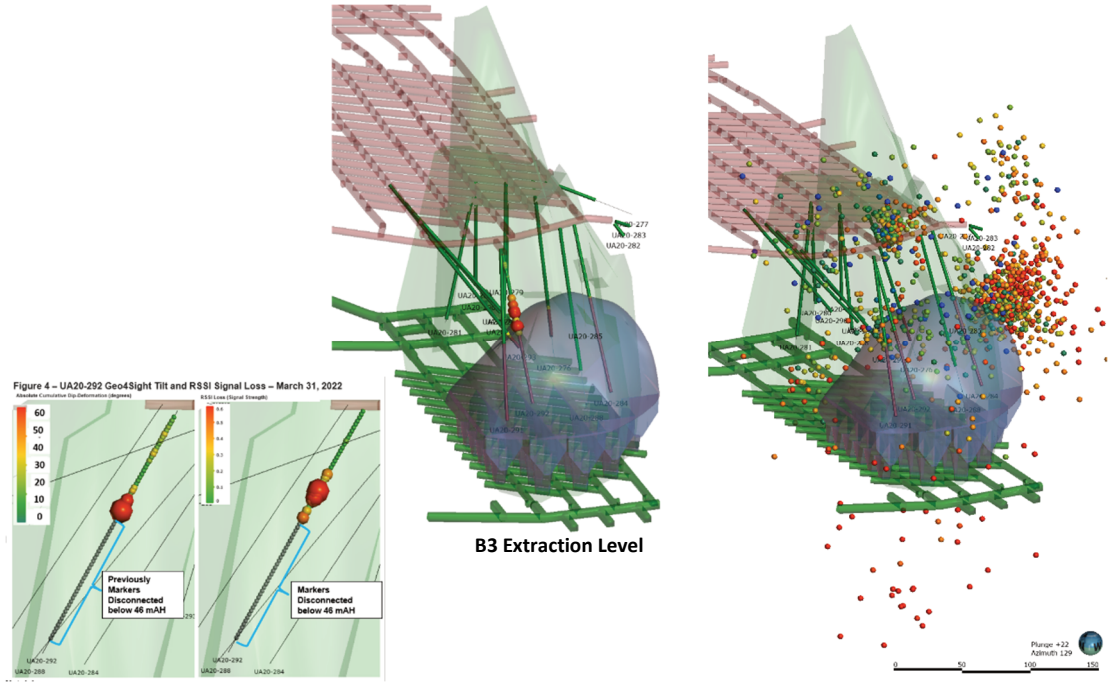

Figure 4 (a) Isometric view of the B3 Cave profile, showing MTDR/OTDR strings, and an example of Elexon Geo4Sight tilt shown as spheres; (b) Seismic events for the month of February 2022

Numerical modelling is also externally completed to assist with cave profile forecasting and comparison to the cave profile generated with instrumentation (Figure 5).

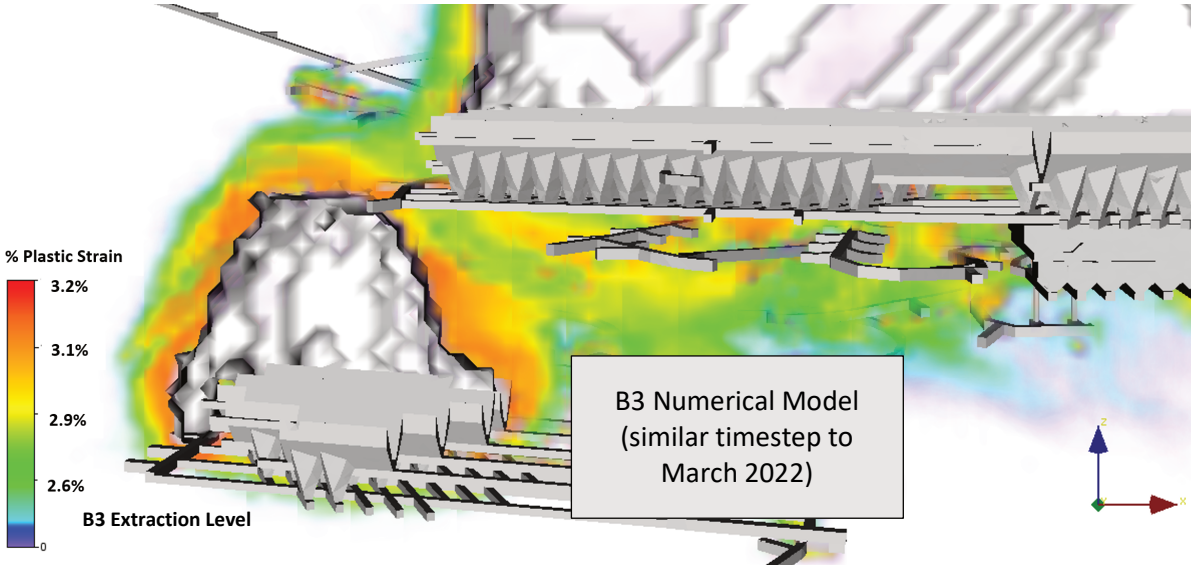

Figure 5 Numerical model (Beck 2021) B3 Cave for 2022 time frame, plotted with percent plastic strain

4 Results and discussion

4.1 Seismic event frequency and production rates

The dataset is divided into two timeframes for the B3 Cave, this is based on instrumentation data interpretation of pre-caving and steady state cave production of B3 (Figure 6):

- Pre-caving: Development of undercutting and initial drawpoints pre-caving (December 2021).
- Caving: Steady state cave production achieved, after HRCrit (January 2022 to March 2022).

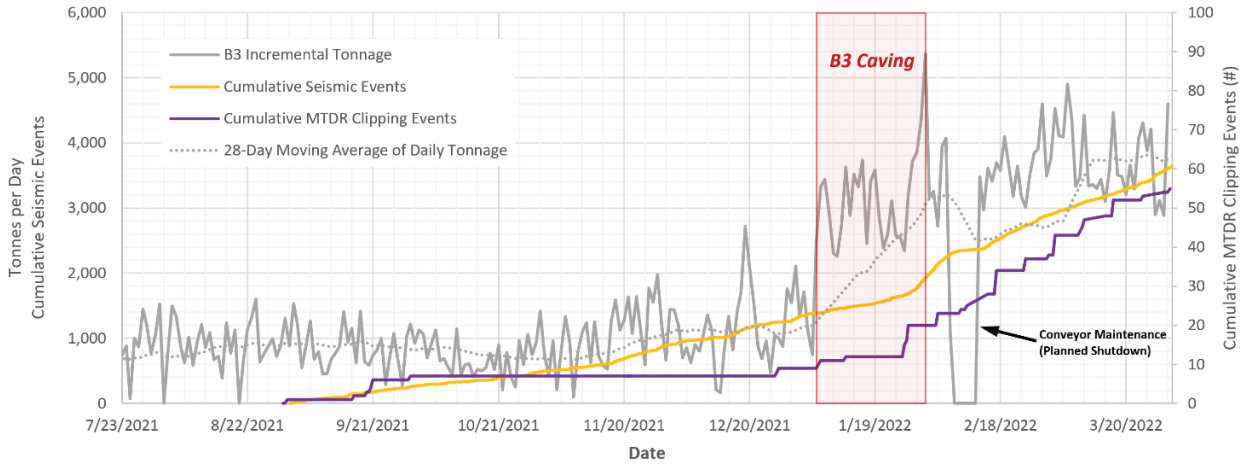

Figure 6 Cumulative MTDR clipping events and seismic events versus B3 incremental tonnage. Conveyor maintenance shutdown between 7th and 12th February 2022

4.2 Seismic tomography results

Passive tomography vertical cutting plane heatmaps (Figure 7) were created through the centre of the expected cave for the pre-caving time frame (September to December 2021), with observations of higher Vp around the initial undercutting and drawpoint blasting. Seismic events for this period are localised to the high Vp undercutting front with a sparse number of seismic events observed above the undercutting and interpreted cave profile.

During January 2022 after HRCrit was met and the mine production ramped up, an increase in seismic response was observed vertically above the cave profile growing progressively shallower throughout the month, while the passive tomography data shows a decrease in Vp vertically but an increase in Vp advancing east as the cave front continues to progress.

In the following months, February and March 2022 continue this trend of increasing Vp values for the advancing cave front (assumed induced cave stresses on intact rock mass) with a decrease in Vp values (assumed as yielding and caved rock mass) following the vertically growing cave profile. The seismic data for these two months corresponds to vertical growth and widening of the cave profile above and around the lower Vp zones and fewer seismic events in advance of the undercut, potentially due to the changes in lithology and faults parallel to the cave advancement east. It is noted that the tomography results can show values in regions where there are very few or no seismic locations as long as there are sensor event raypaths passing through this location.

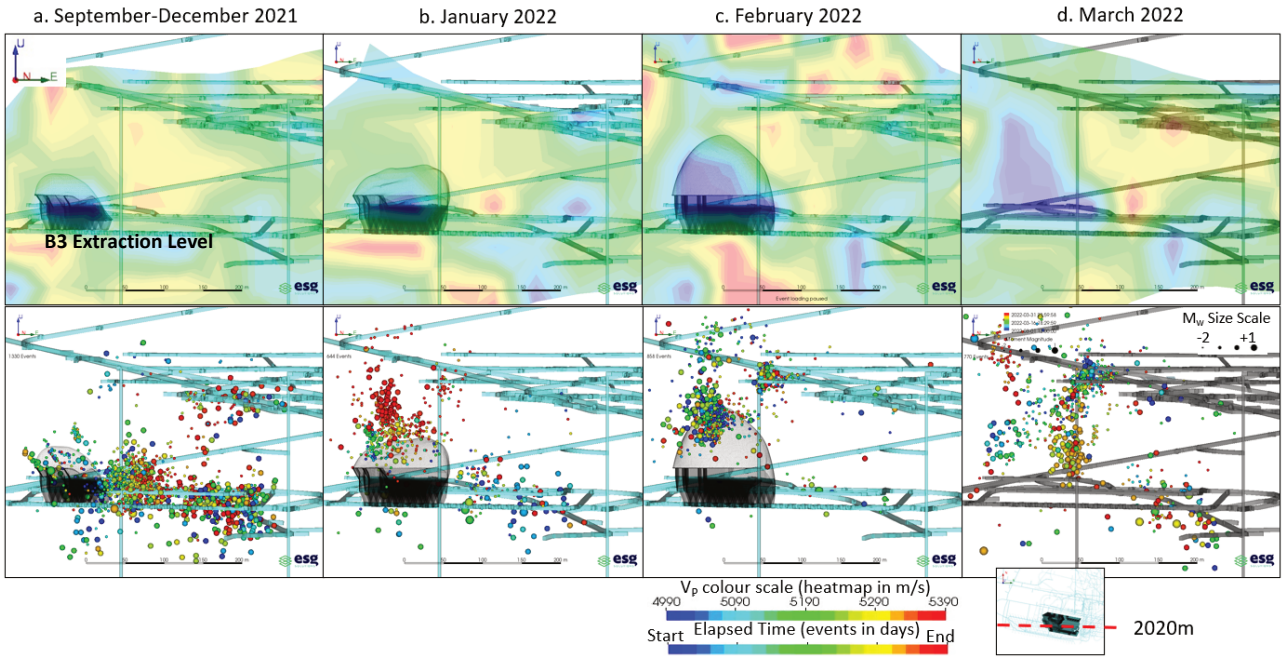

Figure 7 Passive tomography over time with (a) Pre-caving, moving towards the critical hydraulic radius span required for propagation of caving, stress loading observed around cave abutment (b) Caving, cave growth produces stress loading below and above to the east of the cave, (c) Stress loading below and upper west side of cave, (d) Stress loading observed east of cave, with stress relaxation above the cave to the west (cave profile not shown to more clearly observe the low Vp zone)

The low Vp values where caving is taking place above the extraction level can be clearly seen in all time periods for Figure 7, aiding with interpreting the yielding and caved rock mass from mining.

The reader should note the reasonable correlation between the numerical modelling (Figure 5) and the tomographic results (Figure 7) in terms of overall rock mass stress conditions based on the expected cave profile. These results provide New Afton ground control personnel and mine management some confidence in both the numerical modelling and the tomographic results at this time and moving forward.

4.3 Decision-making and conclusions

For the time periods shown in Figures 7b to 7d, a low Vp zone is clearly observed above the extraction level. Aligning this observation with the caving conceptual model, the lowest Vp zone is interpreted to be the caved zone which then transitions to higher Vp values through the zone of loosening into the seismogenic zone and into the pseudo-continuous domain (Figure 8b). A 3D isometric shape is exported of the lower Vp zone (~Vp = 5,090 m/s) to be utilised in interpreting the cave profile (Figure 8a).

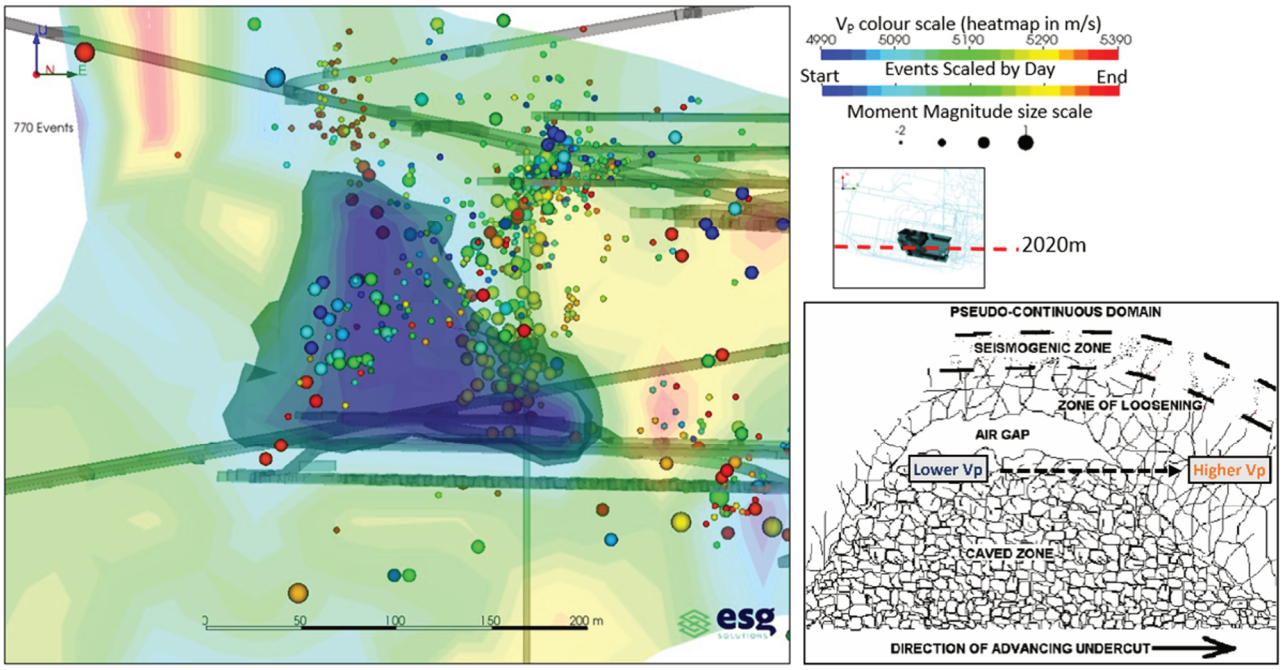

Figure 8 (a) The low Vp outline in the March 2022 tomography heatmap (taken from Figure 6d) provides an interpretable outline, shown with overlaid 3D isosurface (~Vp = 5,090 m/s) and the March 2022 seismic events, (b) Caving conceptual model (modified after Duplancic and Brady 1999), interpreting the correlation of lower to higher Vp

Seismic tomography can be a useful tool to compliment the other instrumentation data when interpreting the cave profile, allowing for the mine operations team to further understand and mitigate caving related risks. The isosurface generated by filtering the low Vp in the area of active B3 caving provides an interpretable outline that could not be determined by using seismic event locations. As B3 Cave progression develops at New Afton, a Vp outline is interpreted monthly and utilised to monitor the cave profile development in compliment to the seismic event locations, MTDR and OTDR), and Elexon Geo4Sight and beacons. An example for the month of March 2022 is seen in Figure 9.

In addition, the fact that the seismic tomography observed in Figure 7d also corroborates reasonably with the numerical modelling analyses (Figure 5) in terms of stress changes in the rock mass is comforting and indicates that the B3 Cave is behaving as expected to date. The seismic tomography analyses add a new dimension to aid rock mechanics and mining decisions and will help interpret the cave profile for areas between other fixed location instrumentation installed as part of the monitoring program at New Afton.

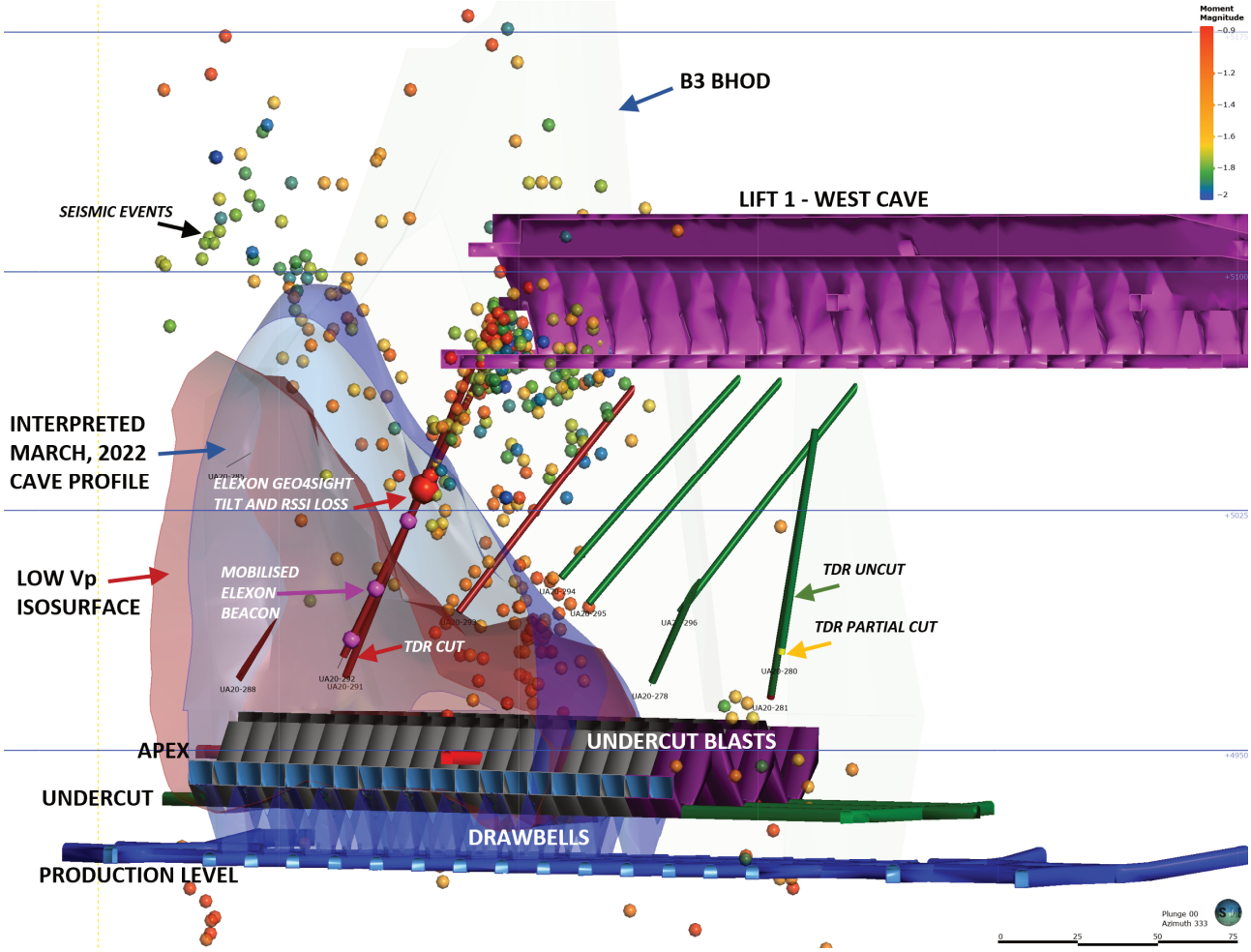

Figure 9 3D section iso view of the interpreted cave profile for March 2022 using Elexon Beacons, Elexon Geo4sight, optical and metallic TDR, and March 2022 seismic events. Note that the isometric and transparent view and cross-section width appear to show a number of seismic events within the cave profile. This is however not occurring, but is an artefact of the viewing angle

Acknowledgement

The authors thank New Gold, New Afton Mine for the support of this paper and Kevin Davenport from Knight Piésold for assisting with processing TDR and Elexon instrumentation data.

References

Afrouz SG & Westman, EC 2018, 'Review and simulation of passive seismic tomography in block cave mining', in Y Potvin & J Jakubec (eds), *Caving 2018: Proceedings of the Fourth International Symposium on Block and Sublevel Caving*, Australian Centre for Geomechanics, Perth, pp. 223–230.

Baig, AM, Bosman, K & Urbancic, TI 2017, 'Temporal changes in stress state imaged through seismic tomography', in J Wesseloo (ed), *Proceedings of the Eighth International Conference on Deep and High Stress Mining*, Australian Centre for Geomechanics, Perth, pp. 269–274.

Beck 2021, New Afton Mine internal document.

Carlson, SR & Young, RP 1993, 'Acoustic emission and ultrasonic velocity study of excavation-induced microcrack damage at the Underground Research Laboratory, *International Journal of Rock Mechanics and Mining Sciences & Geomechanics Abstracts*, vol. 30, no. 7, pp. 901–907.

Collins, DS, Pinnock, I, Shumila, V, Trifu C-I, Kamp, C, Davies, A & Chan, A 2013, 'Optimizing microseismic source event location by applying a variable velocity model to a complex geological and mining setting at the New Gold Afton block cave', in F Hassani (ed), *Proceedings of the 23rd World Mining Congress on Advances in Mining Engineering*, Montreal, PDF paper 674, published by CIM.

Crowley, JW, Baig, A & Urbancic, T 2015, '4D tomography and deformation from microseismic data', *Proceedings of the 85th Annual Meeting of the Society of Exploration Geophysics*, Society of Exploration Geophysicists, Tulsa.

De Beer, W, Ardito, JA, Mercier, J-P & Falmagne, V 2012, 'Beyond coloured balls – making sense of large volumes of microseismic data with diverse source mechanisms', in Y Potvin (ed), *Deep Mining 2012: Proceedings of the Sixth International Seminar on Deep and High Stress Mining*, Australian Centre for Geomechanics, Perth, pp. 149–159.

De Beer, W, Smith-Boughner, L, Viegas, G, Bosman, K & Angus, D 2018, 'Towards physics-based hazard assessment tools for developing blanket re-entry rules', in Y Potvin & J Jakubec (eds), *Caving 2018: Proceedings of the Fourth International Symposium on Block and Sublevel Caving*, Australian Centre for Geomechanics, Perth, pp. 545–552.

Duplancic, P & Brady, BH 1999, Characterisation of caving mechanisms by analysis of seismicity and rock stress. Proceedings of the 9th ISRM Congress, Paris, France, International Society for Rock Mechanics, pp. 1049–1053.

Ma, X, Westman, E, Counter, D, Malek, F & Slaker, B 2020, 'Passive seismic imaging of stress evolution with mining-induced seismicity at hard-rock deep mines', *Rock Mechanics and Rock Engineering*, vol. 53, pp. 2789–2804.

Maxwell, SC & Young, RP 1996, 'Seismic imaging of rock mass responses to excavation, *International Journal of Rock Mechanics and Mining Sciences & Geomechanics Abstracts*, vol. 33, no. 7, pp. 713–724.

Mercier, J-P, de Beer, W, Mercier, J-P & Morris, S 2015, 'Evolution of a block cave from time-lapse passive source body-wave travel time tomography', Geophysics, vol. 80, no. 2, pp. WA85–WA97, https://dx.doi.org/10.1190/geo2014-0155.1

Pfitzner, MJ, Westman, E, Morgan, M, Finn, D & Beck, DA 2010, 'Estimation of rock mass changes induced by hydraulic fracturing and cave mining by double difference passive tomography', in Y Potvin (ed), *Proceedings of the Second International Seminar on Block and Sublevel Caving*, Australian Centre for Geomechanics, Perth, pp. 677–684.

Viegas, G, Bosman, K, Angus, D, de Beer, W & Urbancic, T 2018, 'Mapping cave front growth utilising the collective behaviour of seismicity and velocity fields', in Y Potvin & J Jakubec (eds), *Caving 2018: Proceedings of the Fourth International Symposium on Block and Sublevel Caving,* Australian Centre for Geomechanics, Perth, pp. 577–588.

Westman, E, Luxbacher, K & Swanson, PL 2008, 'Local earthquake tomography for imaging mining-induced changes within the overburden above a longwall mine', *Proceedings of the 42nd US Rock Mechanics Symposium*, ARMA, SanFrancisco, pp. 1077–1083.

Westman, E, Luxbacher, K & Schafrik, S 2012, 'Passive seismic tomography for three-dimensional time-lapse imaging of mining-induced rock mass changes', *The Leading Edge*, vol. 31, pp. 338–345.

Young, R & Maxwell, S 1992, 'Seismic characterization of a highly stressed rock mass using tomographic imaging and induced seismicity', *Journal of Geophysical Research*, vol. 97, pp. 12361–12373.